LJMU Research Online

Molinari, S, Noriega-Crespo, A, Bally, J, Moore, TJT, Elia, D, Schisano, E, Plume, R, Swinyard, B, Giorgio, AMD, Pezzuto, S, Benedettini, M and Testi, L

 Large-scale latitude distortions of the inner Milky Way Disk from the Herschel/Hi-GAL Survey

http://researchonline.ljmu.ac.uk/id/eprint/5388/

Article

For more information please contact researchonline@ljmu.ac.uk

Large-scale latitude distortions of the inner Milky Way Disk from the Herschel/Hi-GAL Survey.

S. Molinari[1], A. Noriega-Crespo[2], J. Bally[3], T. J. T. Moore[4], D. Elia[1], E. Schisano[1], R. Plume[5], B. Swinyard[6], A. M. Di Giorgio[1], S. Pezzuto[1], M. Benedettini[1], and L. Testi[7,8]

[1] INAF- Istituto di Astrofisica e Planetologia Spaziale, Via Fosso del Cavaliere 100, I-00133 Roma, Italy e-mail: `molinari@iaps.inaf.it`
[2] Space Telescope Science Institute, 3700 San Martin Dr., Baltimore, 21218 MD, USA
[3] Center for Astrophysics and Space Astronomy, University of Colorado, Boulder, 80309 CO, USA
[4] Astrophysics Research Institute, Liverpool John Moores University, Liverpool Science Park Ic2, 146 Brownlow Hill, Liverpool L3 5RF, UK
[5] Department of Physics & Astronomy, University of Calgary, Canada
[6] STFC, Rutherford Appleton Labs, Didcot, UK
[7] European Southern Observatory, Karl Schwarzschild str. 2, 85748 Garching, Germany
[8] INAF-Osservatorio Astrofisico di Arcetri, Largo E. Fermi 5, 50125 Firenze, Italy

Received ; accepted

ABSTRACT

Aims. We use the *H*erschel Hi-GAL survey data to study the spatial distribution in Galactic longitude and latitude of the interstellar medium and of dense, star-forming clumps in the inner Galaxy.

Methods. We assemble a complete mosaic of the inner Galaxy between $l = -70°$ and $+68°$ in the far-infrared continuum from Hi-GAL. The peak position and width of the latitude distribution of the dust column density is analysed by fitting a polynomial function to the diffuse IR surface brightness in 1° longitude bins and the result is compared to MIPSGAL 24-μm data. The latitude distribution of number density of compact sources from the band-merged Hi-GAL photometric catalogues is also analysed as a function of longitude.

Results. The width of the diffuse dust column density traced by the Hi-GAL 500-μm emission varies across the inner Galaxy, with a mean value of $1°.2-1°.3$, similar to that of the distribution of MIPSGAL 24-μm sources and of Hi-GAL sources with a 250-μm counterpart. Hi-GAL sources with a 70-μm counterpart define a much thinner disk, with a mean FWHM~0°.75, in excess of the result obtained by the ATLASGAL submillimetre survey. The discrepancy with the 250-μm source distribution can be explained by relatively higher confusion in the *H*erschel data in the midplane region. The peak of the average latitude distribution of Hi-GAL sources is at $b \sim -0°.06$, coincident with the results from ATLASGAL. The detailed latitude distribution as a function of longitude shows clear modulations, both for the diffuse emission and for the compact sources. The displacements are mostly toward negative latitudes, with excursions of ~0°.2 below the midplane at $l \sim +40°$, $+12°$, $-25°$ and $-40°$. The only positive bend peaks at $l \sim -5°$. No such modulations can be found in the MIPSGAL 24μm or WISE 22μm data when the entire source samples are considered; modulations in part similar to the ones exhibited by the Herschel sources appear when the mid-infrared catalogues are filtered according to criteria that preferentially select YSOs.

Conclusions. The distortions of the Galactic inner disk revealed by *H*erschel confirm previous findings from CO surveys and HII/OB source counts but with much greater statistical significance and are interpreted as large-scale bending modes of the Plane. The lack of similar distortions in tracers of more evolved YSOs or stars rules out gravitational instabilities or satellite-induced perturbations, as they should act on both the diffuse and stellar disk components. We propose that the observed bends are caused by incoming flows of extra-planar gas from the Galactic fountain or the Galactic halo interacting with the gaseous disk. Stars, having a much lower cross-section, decouple from the gaseous ISM and relax into the stellar disk potential. The timescale required for the disappearance of the distortions from the diffuse ISM to the relatively evolved YSO stages are compatible with star-formation timescales.

Key words. Stars: formation - (ISM:) dust - Galaxy: disk - Galaxy: structure - Infrared: ISM

1. Introduction

The detection of low-amplitude "corrugations" in the disk of the Milky Way, within the radius where the full HI warp starts to develop, dates back at least to Gum et al. (1960), who found that the inner Galactic disk, while very flat, contains localised excursions of around 20 pc from the principal Plane of the Galaxy. Quiroga (1974) reported large-scale latitude modulations in the distribution of the HI emission and OB associations as a function of longitude. This result was confirmed by Lockman (1977) and, specifically for the Milky Way Central Molecular Zone, by Liszt & Burton (1980). Such corrugations have also been re-

ported for the disks of other spiral galaxies, e.g., by Matthews & Uson (2008) for IC 2233, with a more pronounced amplitude for HII regions and the star-forming component in general, and basically undetectable in the older stellar component traced by mid-IR continuum radiation. More recently, McClure-Griffiths et al. (2012) used higher-quality radio data to confirm the scenario proposed by Liszt & Burton (1980) of an HI distribution in the CMZ organised in a tilted elliptical disk with an inclination ~24°.

It has been suggested that macroscopic disk distortions, such as the HI warps commonly seen in spiral galaxies as well as in

the Milky Way, may be caused by the gravitational action of orbiting dwarf satellites, like the Magellanic Clouds in the local system. Close passages or minor mergers of the dominant galaxy with such minor systems may well have produced warps (e.g., Sagittarius A in the case of the Milky Way). Although HI warps generally occur in the external regions of spiral galaxies, beyond the radius of the stellar disk, N-body modelling by Edelsohn and Elmegreen (1997) predicted that a satellite the size of the LMC can also generate height and perpendicular velocity perturbations in the inner disk. On the other hand, Weinberg (1991) concluded that only long-wavelength modes such as the Galactic warp would be excited by such interactions. In addition, Pranav & Jog (2010) showed that the Galactic potential in the inner regions of the disk is intense enough to suppress the development of perturbations induced by dwarf satellites, while the perturbation would be free to fully develop into the observed large-scale warps only at larger radii where the stellar density drops.

The observed structures may, however, be more than just interesting details of the mechanics of spiral galaxies and may in fact be related to the star-formation process. Alfaro et al (1992) have suggested that corrugations seen in the Sagittarius-Carina arm are related to spatially correlated enhancements in star-formation activity, with a causal connection via 3D waves and the growth of gravitational and magnetic instabilities. Franco et al. (1988) investigated the possibility that impacts on the Galactic Plane by High-velocity Clouds (HVCs) may explain the high latitude of the Orion and Monoceros star-forming regions. The effect of magnetic fields was added by Santillán et al. (1999), the conclusion of which was that the HVC gas does not penetrate the inner disk but can induce oscillations and trigger Parker instabilities. Such interactions may result in significantly enhanced gas densities in previously magnetically subcritical clouds (Vaidya et al. 2013). The Parker instability itself may give rise to undulations in spiral arms in both the azimuthal and vertical directions, and in the *z*-component of the velocity, while also producing very large gas concentrations with masses similar to those of HI super clouds in the Galaxy (Franco et al. 2002).

What is generally termed "Galactic fountain" gas, is Galactic ISM material pushed out of the Plane with sufficient momentum by supernova explosions in OB associations, that then falls back onto the Plane after cooling (Spitzer 1990), perhaps in the form of HVCs, as suggested by Bregman (1980) and Kwak et al. (2009).

Accretion onto galaxies from halo gas, either from gas stripped from orbiting dwarf galaxies or accretion from a diffuse halo, is commonly invoked to solve the gas depletion problem in star-forming galaxies (e.g., Sancisi et al. 2008). Peek (2009) simulates gas accretion from different sources in the Galactic potential and concludes that accretion from a diffuse halo is able to channel fresh ISM onto the most currently active star-forming Galactocentric radii, while accretion of gas stripped from dwarf satellites would be dominant outside the Solar circle, therefore requiring efficient inward gas radial transport. Although the latter is possible in principle, the need to transfer angular momentum outward would seem to make the process very inefficient, even in the presence of well developed spiral arms (e.g., Peek 2009). In addition, Marinacci et al. (2010) model the effect of the passage of fountain gas through hot coronal gas, and find that this can cause the latter to condense and cool locally to provide an adequate gas supply rate.

While the effects of these phenomena are clearly fundamental to the maintenance of star formation in the Galaxy, the direct detection of this inflowing gas is still elusive. The high-latitude clouds revealed in HI (Wakker & van Woerden 1991) and in the

infrared continuum and CO line emission (Blitz et al. 1984; Weiland et al. 1986) may be participating in this, but it is not at all clear to what extent they provide a reliable estimate of the entire budget of diffuse outer gas currently accreting onto the Milky Way. One possibility would be to reveal these accreting gas flows indirectly through their dynamical effects on the Galactic disk. Given the cross sections involved, the effects should be more detectable on the diffuse component of the disk. The latest generation Galactic Plane surveys in the infrared and submillimetre provide ideal datasets to analyse the large-scale morphological properties of the disk in its diffuse and cold ISM phase.

The numerical magnitude of the Hi-GAL source catalogues with respect to previous submillimetre surveys like the Bolocam Galactic Plane Survey (BGPS Rosolowsky et al. 2010) or ATLASGAL (Contreras et al. 2013; Csengeri et al. 2014), allows us to analyse the latitude distribution of sources with unprecedented detail and statistical significance as a function of longitude. Furthermore, the sensitivity of the *Herschel* PACS and SPIRE cameras coupled with optimal map-making image reconstruction developed for Hi-GAL (Traficante et al. 2011; Piazzo et al. 2012) allows us to also characterise in great detail the latitude distribution of the diffuse emission from the Galactic ISM. The analysis below is based on the first release of Hi-GAL maps and photometric catalogues of compact sources in which the large majority has sizes from point-like to twice the instrumental beam (Molinari et al. 2015). Additional processing done here is the production of multi-tile mosaics for the SPIRE 500-μm band to allow precise quantitative measurement of the latitude distribution of the ISM thermal dust emission. This step was carried out using the new Unimap (Piazzo et al. 2015) software and represents an upgrade of the Hi-GAL pipeline that will be used for further data releases.

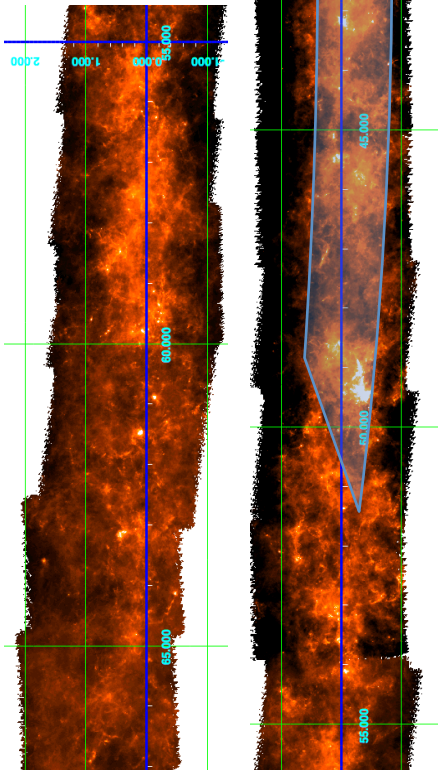## 2. The panoramic view of the inner Galaxy.

Fig. 1: **a**) 500-μm panoramic mosaic of the Galactic Plane for the longitude range $54° \leq l \leq 67°$ (upper panel) and $23°.5 \leq l \leq 56°$ (lower panel). The longitude and latitude scales are given in the figures. The horizontal blue line marks $b=0°$, while the green-line grid marks intervals of 5° in longitude and 1° in latitude. The lightly shaded areas are intended to visually emphasise the slow latitude modulations of the overall dust thermal emission.

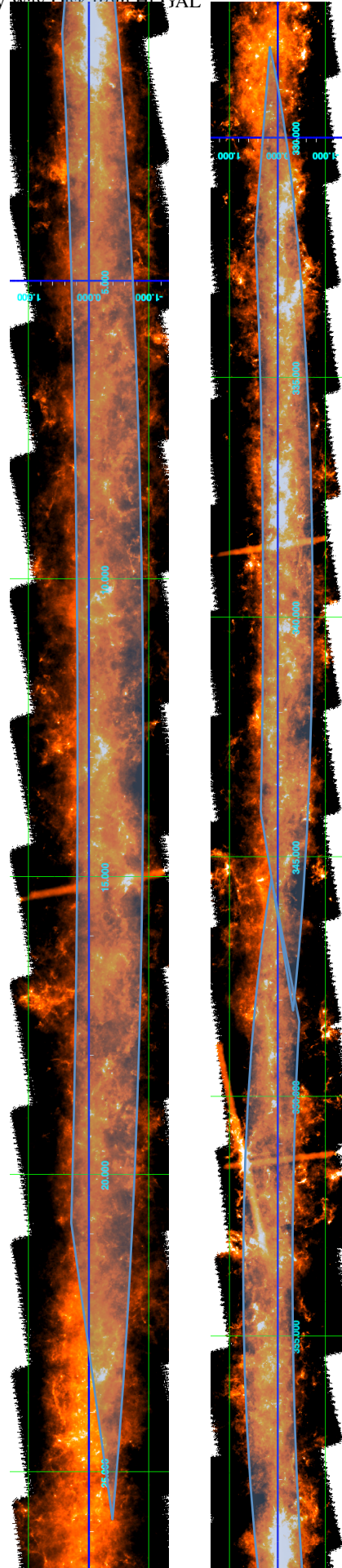Fig. 1: **b**) As fig. 1a, but for the longitude ranges $0° \leq l \leq 27°$ (upper panel) and $327° \leq l \leq 360°$ (lower panel), encompassing the range spanned by the Galactic Bar.
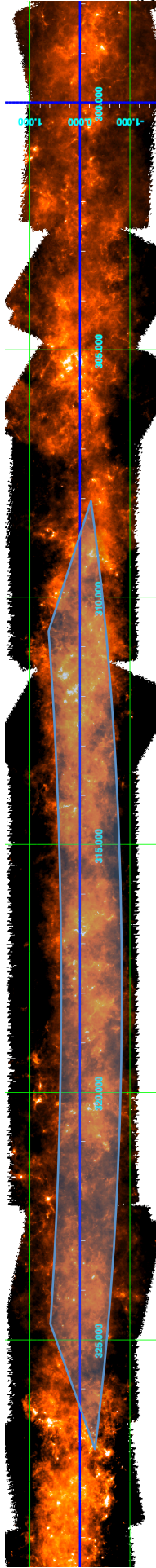
Fig. 1: *c*) As fig. 1c, but for the longitude range $298° \leq l \leq 329°$.
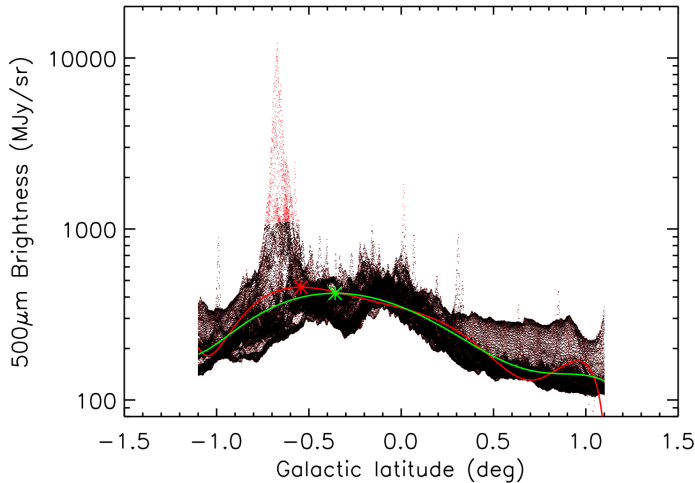
Fig. 2: 500-μm brightness values (all the points) as a function of Galactic latitude in the longitude interval $14°.5 \leq l \leq 15°.5$ from the map in fig. 1b (this longitude range contains M16, which is clearly visible as the large bump at $b \sim -0°.7$). The red thick line is the 7th-order polynomial fit to all points, and the red points are those that are clipped away as they lie above 3 times the r.m.s. of the residuals (after subtracting the fit). The green thick line is the 5th-order polynomial fit to all points that survived this clipping (all the black points). The thick crosses mark the positions of the maxima of each respective fit.

2.1. The latitude distribution of the diffuse ISM.

In fig. 1a, b and c, we present panoramic mosaics of the Hi-GAL 500-μm emission, together covering most of the inner Galaxy surveyed by *Herschel* and subject of the present initial data release. These panoramic views are extremely useful to get a qualitative impression of the latitude distribution of the dust thermal emission and identify systematic patterns. These 500-μm panoramic mosaics can also be used in a quantitatively more rigorous way by estimating the latitude of the centroid emission as a function of longitude. Since bright source complexes (large starforming regions) that could be offset with respect to the overall emission distribution (see, e.g., M16/M17 in fig. 1b would bias the estimate of an overall Galactic Plane centroid of emission, the first step is to clip away these complexes. We first subdivide the image in bins of 1° amplitude in longitude and, using a 7th-order polynomial, fit the brightness values of all pixels in each longitude bin as a function of latitude (thick red line in fig. 2, where we illustrate the particular case of the 1° bin centered at $l = 15°$ that contains M16).

We then compute the r.m.s. of the residual distribution and clip away all pixels whose brightness exceeds this r.m.s. by more than a factor of three (the red points in the same figure). The polynomial order 7 was found, based on trial and error on several locations in the Plane, to be a satisfactory compromise for representing the large and medium-scale components of the diffuse emission (qualitatively $\delta \geq 10'$) but not the brightest and small-scale source clusters. The remaining pixels are again fitted as a function of latitude, this time with a 5th-order polynomial, and the maximum of the fit was assumed as the centroid of the emission. To characterise the latitude width of the emission band we derived the latitude values where the fit reaches the 50% value relative to its maximum. Again, the choice of this functional form was made after experimenting in detail over several locations in the Galactic Plane. The latitude distribution of the
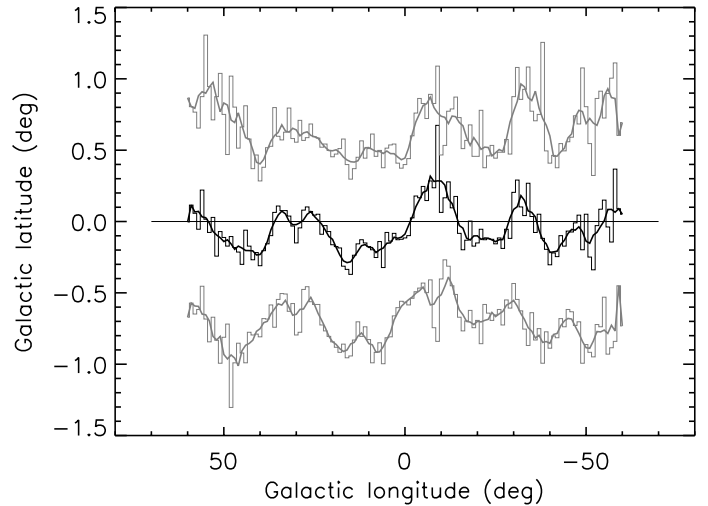

Fig. 3: Distribution in Galactic longitude of the latitude values for the centroid (black histogram) and the upper and lower 50%-level values (grey histograms) of the 500-μm emission (see text for a detailed explanation). The thick lines represent the smoothing of the distributions with a 5°-wide running boxcar.

observed 500-μm flux appears heavily skewed, which dissuaded us from using a Gaussian fit; the 5th-order polynomial appeared to be the best compromise between obtaining a reliable indication of the overall distribution peak, without being too sensitive to small-scale structures. Fig. 2 shows that this simple method is effective in estimating the latitude centroid of the diffuse emission (the green cross in the figure). The longitude distribution of the emission latitude centroid, as well as of the latitudes of its 50% levels (above/below), are reported in fig. 3.

2.2. The latitude distribution of Hi-GAL sources.

As an additional tool to characterise the vertical distribution of the cold dust in the Galactic Plane as a function of Galactic longitude, we determine the overall latitude distribution of the compact sources found in Hi-GAL. For this, we compute the median value of the Galactic latitudes of all Hi-GAL sources in longitude bins of 1°, limited to those sources that have a counterpart in at least three adjacent *Herschel* bands. This criterion is adopted to select sources with a relatively high degree of reliability (see Elia et al. 2015) in the Hi-GAL photometric catalogues of Molinari et al. (2015), resulting in nearly 100 000 sources in the longitude range considered in the present paper. In fig. 4 we plot these median latitude values as a function of longitude for sources with a 70-μm and a 250-μm counterpart as the blue and green histograms, respectively. By construction, all considered sources have a counterpart at 250 μm (this being the central Hi-GAL band). Sources with a 70-μm counterpart therefore form a subset (nearly 23%) of the entire sample. To emphasise large-scale trends, we also show the same distributions smoothed with a 5-bin wide boxcar (thick lines with the same respective colour).

It can be seen that the latitude distribution of the two classes of sources traced by *Herschel* is very similar over the entire longitude range plotted in fig. 4, implying that the 70-μm-counterpart subsample does not depart from the overall behaviour, with three exceptions. The first discrepancy is visible in the 1st quadrant at $50° \leq l \leq 40°$, where the negative bend shown by the 250-μm-counterpart sources is not followed by the 70-μm sources. Looking at fig. 1a, we note that, in this longi-
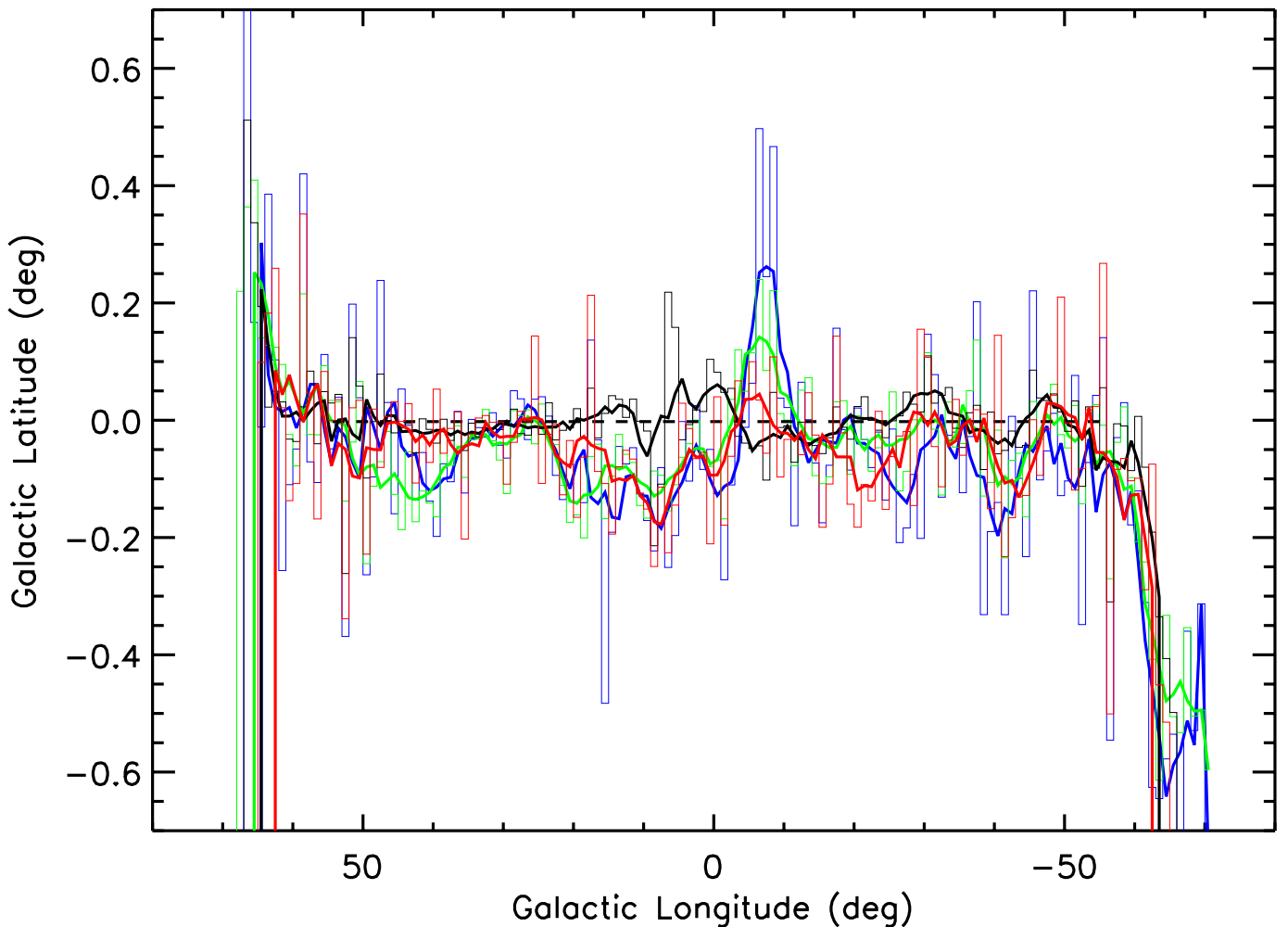
Fig. 4: Histograms representing the distribution of the median Galactic latitude of the Hi-GAL sources detected at $70\,\mu$m (blue line) and at $250\,\mu$m (green line), each with counterparts in at least two adjacent bands. The histograms are computed in $1°$ longitude bins, together with the analogous distribution of entire sample of MIPSGAL 24-μm sources (black line); the distribution of the subsample of MIPSGAL 24μm sources selected by Robitaille et al. (2008) using color criteria targeted toward YSOs is shown with the red line. The thick coloured lines show the result of a $5°$-wide running boxcar smooth. The horizontal dashed black line reports the median latitude of all MIPSGAL 24-μm sources that essentially coincides with the nominal $b=0°$ midplane.

tude range, the overall diffuse emission is clearly bending toward negative latitudes but there are discrete, large, star-forming complexes like those at $l \sim 46°.5$ and $l \sim 43°$ at latitudes close to $b=0°$. Billot et al. (2011) carried out a detailed study of the clustering properties of Hi-GAL compact sources detected toward the $l=59°$ and $l=30°$ Galactic Plane fields, showing that the 70-μm sources have a higher degree of clustering in HII-region complexes than sources detected at $250\,\mu$m. It is therefore not surprising that the latitude distribution of 70-μm sources may be heavily biased by the presence of star-forming complexes. The second discrepancy between the median latitude of 70-μm and 250-μm sources is found at $-5° \leq l \leq -10°$ in fig. 4, where the smoothed 70-μm distribution peaks at much higher latitudes. Again, the presence of prominent star-forming regions biases the 70-μm source distribution; in this case it is the NGC6334/6357 complexes, as it can be easily verified in fig. 1b. The third discrepancy is found at $-23° \leq l \leq -30°$ in fig. 4, where the 70-μm source median latitude suddenly drops to $b \sim -0°.3$ in 4–5 histogram bins, while the 250-μm median stays closer to $b \sim 0°$. This discrepancy is again due to the peculiar distribution of the 70-μm sources in the two giant star-formation complexes

visible in this longitude range: that centered around RCW 106 (Mookerjea et al. 2004), and the complex of HII regions around G330.986-00.433 (Anderson et al. 2014), both of which are concentrated toward the lower boundary of the main Galactic Plane emission band. Again, the rest of the Plane in that longitude range contributes much more in 250-μm sources than it does at $70\,\mu$m.

The reliability of Herschel source counts may be influenced by incompleteness due to confusion from extended dust emission of molecular clouds and diffuse cirrus piling up along the line of sight (Molinari et al. 2015). This prevents fainter sources being detected on top of relatively stronger backgrounds so that source counts at latitudes closer to the midplane, where the more intense background conditions are found, are depressed to an extent that is difficult to quantify. Had we to estimate and apply such correction to source counts, however, this would be higher in regions with relatively higher backgrounds, and this would amplify the results of fig. 4 because the latitude distribution of the detected sources *before the hypothetical correction* already follows the trend of the diffuse emission.

The black histogram and line in fig. 4 report the same quantities computed from the MIPSGAL 24-μm point-source catalogue (Shenoy et al., priv. comm.). Sources from the MIPSGAL 24-μm survey represent a mix between YSOs and star-forming clumps (relatively more evolved, on average, compared to similar objects traced by the Hi-GAL source catalogues), and more evolved MS objects like post-AGB stars (Carey et al. 2009). As a whole, the 24-μm MIPSGAL catalogue traces more evolved objects compared to Hi-GAL; the trend shown in fig. 4 shows a flatter and relatively less structured behaviour with respect to Hi-GAL compact sources, with no indication of latitude modulations similar to those exhibited by the Hi-GAL compact sources. If, however, we use the sources from MIPSGAL that were selected by Robitaille et al. (2008) according to criteria that should result in a sample dominated by YSOs, we obtain (the red line in fig. 4) a distribution that more closely resemble the ones from Herschel. In particular, we mention the downward bends at 25° $\lesssim l \lesssim$ 0°, at $l \sim -20°$ and $l \sim -40°$.

The statistical significance of the median latitude distributions of the Hi-GAL sources is characterised in fig. 5 for the sources with counterparts in the two Hi-GAL bands of fig. 4 in the two panels. The plots show with a full line the absolute value of the smoothed median latitude of the Hi-GAL sources, i.e. the absolute value of the thick lines in fig. 4. The dashed line in fig. 5 reports the running standard deviation of the difference, as a function of the longitude, between the median source latitude and its smoothed function; in essence we computed the standard deviation of the difference between the thin and the thick lines (blue and green) in fig. 4 in a running boxcar 10-degrees wide. The latitude distortions can be assumed significant (at least at the 1σ level) for the longitude ranges where the dashed line is close or above the full line. In addition, we regard as a valid significance indicator the fact that the amplitude of the distortion keeps close to or above its running r.m.s. for several degrees.

3. Results

3.1. The width of the Galactic disk

The amplitude of the latitude distribution of the quantities described above as a function of longitude is reported in fig. 6. The FWHM of the latitude distribution of the 70-μm and 250-μm Hi-GAL sources (blue and green lines), and the MIPSGAL 24-μm sources (black), are determined by fitting a Gaussian to the source latitude distribution in 1° longitude bins. The amplitude of the 50%-level of the Hi-GAL 500-μm diffuse emission (orange) is taken from fig. 3, and it is not the result of a Gaussian fit to the latitude distribution.

The latitude FWHM of the 250-μm sources and of the 500-μm diffuse emission range between 1° and 1°.5, on average, with the latter also showing peaks close to 2°. The width of the Plane in these two tracers varies in a similar way with Galactic longitude. The FWHM of the MIPSGAL 24-μm sources follows a similar trend, with a noticeable departure toward the central molecular zone, possibly also due to the Galactic bulge; however, Herschel/SPIRE data were taken in "bright mode" in the central 6° around the Galactic Centre, to mitigate saturation at the expense of sensitivity, and this may be the origin of the dip in the FWHM of the latitude distributions of both Hi-GAL 250-μm sources and 500-μm diffuse emission. A similar FWHM of the Plane is also reported by Beuther et al. (2012) for the GLIMPSE red sources in the Robitaille et al. (2008) sample.

The distribution of the Hi-GAL 70-μm sources traces a much thinner Plane, with the FWHM showing large variations between
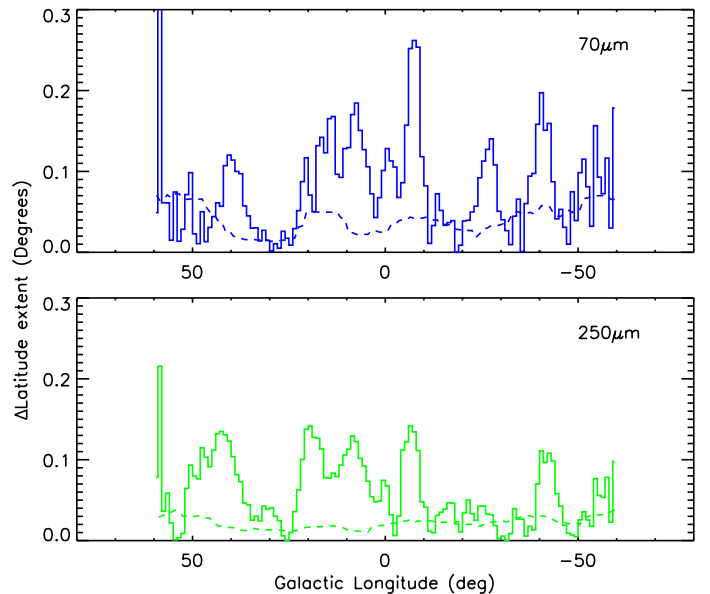

Fig. 5: Full-line histograms representing, as a function of longitude, the absolute value of the smoothed median source latitude (the thick lines of fig. 4), and the running standard deviation (dashed lines) of the residuals between the median latitude and its smoothed function (i.e., the difference between the thin and thick lines in fig. 4), computed using a boxcar of 10 degrees. The upper panel shows the result for the 70-μm sources in blue, and the lower panel shows the 250-μm sources in green. Note that we are using only those Hi-GAL sources with a counterpart in at least 3 adjacent bands.

~0°.3 and 1°.3, with a mean value of 0°.75 for −60°$\leq l \leq$+60°. This is slightly larger than the 0°.6 value reported for the ATLASGAL 870-μm sources by Beuther et al. (2012). The amplitude of the variations in width for the 70-μm sources is larger than for the 250-μm sources, and can be explained by the fact that sources with a 70-μm counterpart trace the prominent star-forming and Hii-region complexes more closely (Billot et al. 2011) and therefore can generate strong local departure from larger-scale longitude trends.

It may seem puzzling that the Hi-GAL 250-μm sources do not show the same latitude distribution as the ATLASGAL 870-μm sources (Beuther et al. 2012), while the Hi-GAL 70-μm sources do. APEX/LABOCA at 870 μm has the same spatial resolution of Herschel/SPIRE at 250 μm, and the wavelengths are both in the Rayleigh-Jeans section of the SED of cold dust, so that one would naively expect the two samples to exhibit a similar behaviour in their statistical distributions. The discrepancy is due to the significantly different sensitivities of the two instruments, coupled with the different completeness limits that can be reached on and off the midplane at 250 μm. In the most recent version of the ATLASGAL source catalogue, Csengeri et al. (2014) report the peak of the 870-μm integrated flux distribution at $\sim$ 0.6 Jy. Extrapolating to 250 μm assuming $\beta = 1.5$, this would correspond to a flux of ~47 Jy. On the other hand, the peak of the 250-μm source integrated flux distribution is at $\sim$ 3 Jy (Molinari et al. 2015), showing that Herschel is, as expected, at least 10 times more sensitive than current top-notch ground-based submillimetre surveys. The ATLASGAL sources therefore represent the highest-flux fraction of the Hi-GAL compact sources, suggesting that the different latitude distributions of the two samples is due to a bias from the different ranges of
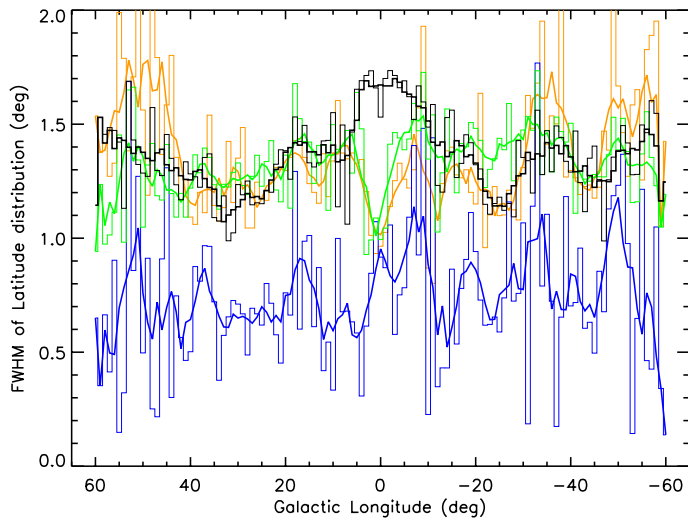
Fig. 6: The distribution as a function of longitude of the Full Width at Half Maximum of the latitude distribution of various quantities described in the text, averaged in 1° longitude bins. The Hi-GAL 70-μm and 250-μm compact sources belonging to the band-merged source list are indicated with full line blue and green histograms, where the FWHMs have been determined by a Gaussian fit to the source latitude distribution in each longitude bin. The black histogram represents the distribution of the MIPSGAL 24-μm sources, computed in the same way as for the Hi-GAL sources. The orange histogram represents the FWHM of the Hi-GAL 500-μm diffuse emission obtained simply as the amplitude of the latitude band encompassed by the 50% levels in fig. 3. For each histogram, the thick lines of the same respective colour show the distributions after smoothing with a 5°-wide boxcar.

fluxes sampled. To verify this, we analyse again the latitude distribution of the Hi-GAL 250-μm sources, using only those above a certain minimum integrated flux. For each choice of this minimum flux, we fit with a Gaussian the latitude distribution of the sources in 1°longitude bins and compute the median of the FWHMs between $-60°$and $+60°$. Fig. 7 reports the resulting median FWHM of the 250-μm sources as a function of the 250-μm minimum flux adopted, and proves that the smaller FWHM of the ATLASGAL source latitudes, with respect to Hi-GAL 250-μm sources, is likely to be a sensitivity effect.

The reason for the different latitude distribution of SPIRE 250-μm sources compared to ATLASGAL sources has then to be sought in the population of relatively faint Hi-GAL sources. Cirrus noise considerably changes as a function of latitude for any given longitude in the inner Galaxy. As a consequence, the flux completeness limits for extracted sources vary too. As shown in fig. 8, the distribution of 250-μm fluxes for sources with $|b| \leq 0°.375$ (half the mean FWHM of the 70-μm source latitude distribution as determined from fig. 6), peaks at about ∼7 Jy (full green line), while sources at larger latitudes peak at ∼4 Jy (dashed green line); the distributions show a clear shift. This means that in the brightest cirrus regions closer to the Galactic midplane we are less efficient (due to confusion noise) in picking up relatively fainter sources. This causes a deficit in the 250-μm source counts in the central latitudes, leading to an artificially shallower distribution. No such effect is present at 70 μm (the blue lines in fig. 8).

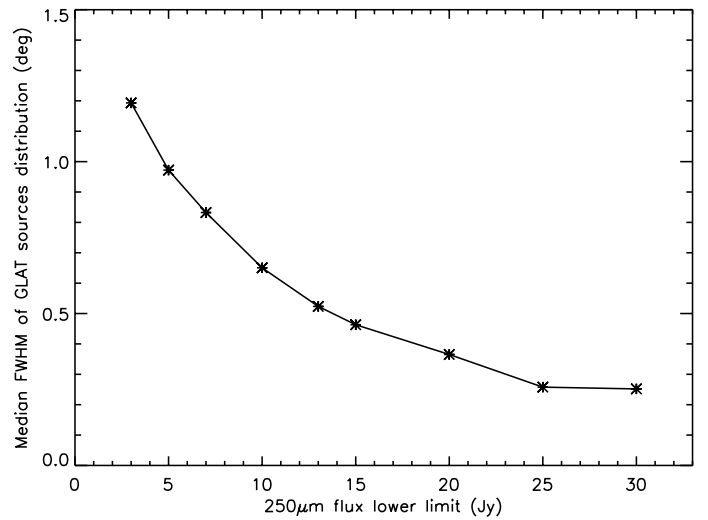Fig. 7: Median values, over the whole longitude range, of the FWHM of the latitude distribution, in bins of 1°, of the 250-μm Hi-GAL sources with integrated flux above a certain limit, as a function of said limit.
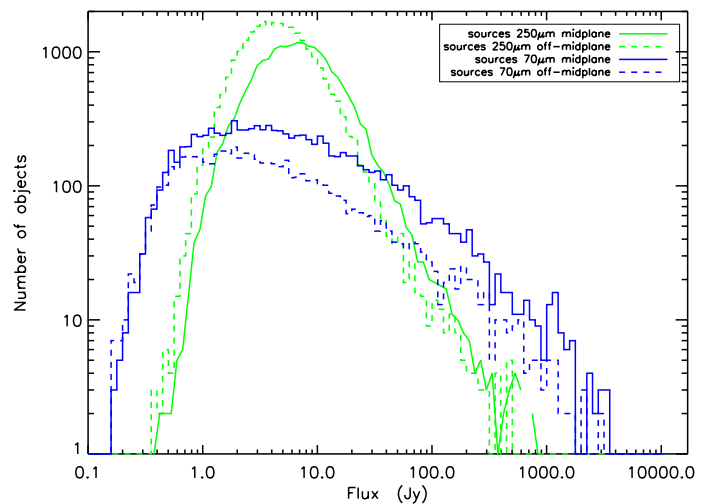

Fig. 8: Flux distribution for Hi-GAL sources at 250 μm (green lines) and at 70 μm (blue lines), for sources with latitudes $|b| \leq 0°.375$ (full lines) and $|b| > 0°.375$ (dashed lines). The value of 0°.375 corresponds to half the mean (over longitude) FWHM of the latitude distribution of the 70-μm sources. Notice the shift in of the 250-μm source distributions for different latitude cuts.

3.2. Large-scale latitude distortions of the dusty Galactic disk

In this section we analyse in detail the latitude distribution of compact sources and diffuse emission from Hi-GAL. We will make extensive use of figures 1, 3, 4 and 5.

3.2.1. The First Quadrant

Fig. 1a shows the emission map at 500 μm in the first Quadrant starting from $l \sim 67°$, where the Hi-GAL coverage starts to climb up in latitude to follow the Galactic Warp. In a popular representation of the four-arm Milky Way Galaxy, the region $60° \leq l \leq 50°$ is dominated by the Local Arm; many noticeable star-forming complexes in this region are located at heliocen-

tric distances of a few kpc at most (e.g., the Vul OB1 complex, see Billot et al. 2010). As soon as we see the distribution of the bulk of the emission coming down from the warped disk onto the $b = 0°$ midplane, at around $l = 60°$, the latitude distribution of the emission appears to be overall centred around the midplane. As we move to smaller longitudes we see that, starting from $l \sim 50°$, approximately corresponding to the tangent point of the Sagittarius Arm, the overall distribution of the 500-μm emission, neglecting local oscillations at the sub-degree scale, begins to be more and more shifted towards lower latitudes. On a purely visual level, it is immediately apparent that the majority of the emission at $50° \geq l \geq 36°$ in fig. 1a is mostly concentrated below $b = 0°$. The curved shaded area superimposed on the map is meant to guide the eye along this downward bend of the overall emission that, after reaching a minimum around $l \sim 40°$, comes up to rejoin the $b = 0°$ midplane at around $l \sim 36°$. The distribution remains centred at $b \sim 0°$ as we proceed to smaller longitudes, where the Scutum-Centaurus Arm starts to dominate, through the W43-G29.9 complex and toward the $l \sim 25°$ region. The negative bend in the latitude distribution of the emission seems therefore confined to the portion of Plane dominated by the Sagittarius Arm. This behaviour for $50° \leq l \leq 36°$ is quantitatively confirmed in fig. 3, where the 500-μm emission centroid is indeed staying consistently below $b = 0°$ for $50° \leq l \leq 36°$, reaching a minimum value of $b \sim -0°.25$. This displacement appears to be significant judging by the dispersion of the centroid histogram (thin histogram) with respect to its boxcar running average (thick black line) in fig. 3.

The same can be seen in the latitude distribution of the compact sources in fig. 4. Here, the amplitude of the latitude dip is relatively smaller (less than $0°.2$), but it is visible both for the 70- and the 250-μm sources. Fig. 5 shows that this bend is significant to about the 2-σ level (blue and green dashed lines are close or well above the full lines). We again note that although the effect is strictly speaking marginal, we are looking at degrees-wide longitude sections where the dashed line stays above the full line. It is interesting to note here that the latitude distribution of the 24-μm compact sources from MIPSGAL does not follow the dip but stays remarkably flat and close to $b = 0°$, even if the Robitaille et al. (2008) YSO-dominated 24μm sample is considered.

3.2.2. The Galactic Bar

Fig. 1b shows in two subpanels a much larger longitude range from $l \sim 27°$, through the Galactic Centre, to $l \sim 328°$. It is dominated by the Scutum-Centaurus arm from its tangent point in the 1st quadrant, the entire Galactic Bar and Central Molecular Zone, and the Norma Arm and its tangent point in the 4th quadrant. At around $l \sim 25°$, the emission distribution that has remained centred on $b \sim 0°$ since $l \sim 36°$ (see previous section) starts again to bend slowly downward. For longitudes smaller than $20°$, the emission is consistently found at negative latitudes; again, the shaded area on the figure is useful to guide the eye along this bend. This is the near side of the Galactic Bar. The emission band starts to climb up again below $l \sim 5°$, goes across the midplane at the Galactic Centre, and up to positive latitudes in the fourth Quadrant. The lower panel of fig. 1b clearly shows that the barycenter of the emission appears consistently above $b \sim 0°$ for longitudes $358° \geq l \geq 345°$ ($-2° \geq l \geq -15°$), corresponding to the far side of the Galactic Bar, approaching again $b \sim 0°$ roughly at the location of the far tip of the Bar. Beyond this location we see again that the emission barycenter heads to negative values until the tangent point of the Norma Arm is reached, at around $l \sim 330°$ (or $l \sim -30°$.).

As in the previous section, the visual impression from the panoramic images is quantitatively verified using the latitude distribution of the 500-μm emission barycenter in fig. 3, as well as the distribution of the median latitude of the compact sources in fig. 4. The figures confirm that the Plane, as traced by both the diffuse 500-μm emission and by the 70- and 250-μm compact sources, stays around $b \sim 0°$ for $35° \leq l \leq 25°$, making a negative latitude bend all the way across the Galactic Centre, coming up to positive latitudes after that until $l \sim -15°$. We believe the evidence is robust because the above trend is also consistently shown by the distribution of the 50% levels of the 500-μm emission (the grey lines in fig. 3), as well as confirmed, with similar shape and magnitude, by the 70-μm and the 250-μm compact-source distribution. The only two locations where the distributions of the 70-μm and 250-μm sources differ is at $l \sim 18°$, where the 70-μm distribution is well above the 250-μm one and goes back to $b \sim 0°$), and at $l \sim -6°$, where the upward climb of the 70-μm sources is much more marked. These two occurrences are due to the local bias in the median estimate of the 70-μm source latitude induced by the large M17 and NGC6334/6357 star-forming complexes. These distortions are significant over the range $+25° \geq l \geq -10°$ at the 7-σ level for the 250-μm sources and at 4–5σ for the 70-μm sources (from fig. 5). For the latter, the r.m.s. of the latitude distribution is larger than the amplitude of the distortion between $20°$ and $15°$, due to the peculiar latitudes of the M16/M17 complexes with respect to the local median. Again, the significance should be judged not only by pure σ levels over the r.m.s., but also based on the persistence of the significance over an area a few degrees wide.

There is an additional downward bend that can be visually identified at $345° \geq l \geq 330°$ in fig. 1b that is also visible in fig. 3 at $-15° \geq l \geq -30°$, although with a lower magnitude compared to the region of the Galactic Bar. The distribution of the 70-μm sources shows the same trend, but the 250-μm one does not and remains centered at $b \sim 0°$. We regard the Plane distortion in this region as less certain. Again, we note how the latitude distribution of the 24-μm compact sources from the entire MIPSGAL sample does not follow any of the patterns exhibited by the diffuse emission or the compact-source distribution in Hi-GAL. The situation is different for the YSO-dominated sample of Robitaille et al. (2008) that instead exhibits the downward bend between $20°$ and $0°$.

3.2.3. The Fourth Quadrant

The appearance of the Plane in the diffuse 500-μm emission in the rest of the 4th quadrant is shown in fig. 1c, where the band of emission is mostly centred at $b \sim 0°$. There is a downward bend at $325° \geq l \geq 315°$ ($-35° \geq l \geq -45°$) that is visible in fig. 3 and in the compact-source distribution in fig. 4. The overall emission along the Plane in this region is more inhomogeneous with respect to the Bar and the 1st quadrant, with gaps of relatively faint emission. The significance of the distorsion patterns seems however reliable. Moving further away from the inner Galaxy, at $l \leq 310°$ (or $l \leq -50°$) the 500-μm Plane emission appears much more widely spread in the vertical direction, which explains the relatively higher level of channel-to-channel noise in figs 3 and 4.

3.3. Characterising biases for the large-scale distortions.

3.3.1. Distance effects

The position of the Sun ~27 pc above the nominal $b = 0°$ Plane has to be considered as one of the possible reasons why the latitude distribution of Galactic sources retrieved in Hi-GAL or in ATLASGAL is generally peaked to slightly negative latitudes (Molinari et al. 2015; Beuther et al. 2012). This effect would, however, also generate distance-dependent distortions, in that closer objects would appear at more negative latitudes than more distant objects. To check if this may be the cause of the observed distortions, we made a preliminary investigation using the subset of Hi-GAL sources for which a heliocentric distance estimate is available and that will be presented by Elia et al. (2015).

The longitude range of the Galactic Plane covered in the release of Molinari et al. (2015) was divided in bins of 1°, and for each bin we computed the distance distribution of the objects along the line of sight in bins of 1 kpc. The distance at which the distribution peaks is likely to provide the major contribution, in terms of source numbers, to the determination of the median source Galactic latitude reported in fig. 4. We find a location at $d \sim 7 - 10$ kpc for the majority of the sources in the $35°\leq l \leq 50°$ longitude range, $d \sim 10 - 13$ kpc for the $12°\leq l \leq 20°$ range (we do not have distance determinations for sources closer to the Galactic Centre at the moment), and $d \sim 1.5 - 3$ kpc for the $340°\leq l \leq 350°$ range. None of these preliminary findings agrees with the expectations for a latitude distortion induced by distance effects.

We therefore conclude that the apparent distortions are real. A more thorough analysis will be needed (Elia et al. 2015) to verify in detail to what extent the distortions are an overall property of the Galactic disk or are confined to specific arm sections.

3.3.2. Source completeness biases in 24μm catalogues

We investigate here the possibility that the shape of the source latitude distributions as a function of longitude as reported in fig. 4 for the entire sample of MIPSGAL 24μm sources (the black line), may be biased by incompleteness in source catalogues due to confusion from extended emission or extinction.

The situation is different for the distribution of MIPSGAL 24 μm sources (the black line in fig. 4); here a possible limitation to the detection of faint sources is extinction by dust. In this case the effect should be higher where the dust column is higher along the Plane, as traced by the 500 μm emission (see figures 1 and 3). The fact that, contrary to what happens for the Hi-GAL 70 and 250 μm sources, the distribution of the 24 μm sources *does not show* the same oscillations in latitude centroid as a function of longitude exhibited by the 500 μm diffuse emission (the black line in fig. 3), could then be due to dust extinction that depresses the 24 μm source counts on the peaks of the 500 μm emission. A way to mitigate this bias effect is to compute the distribution of 24 μm sources only for objects with fluxes above the completeness limit, so that each latitude bin is equally treated providing a less biased median latitude estimate. There is currently no flux completeness limit for the yet unpublished Shenoy et al. catalogue; however, a simple histogram of the fluxes shows a peak around ~ 3 mJy. Since the turn-down of fluxes histograms from photometric catalogues is typically very close to the completeness limit (e.g. Molinari et al. 2015 for the Hi-GAL catalogues) we tentatively assume 3 mJy as an average value for 24 μm completeness in the Shenoy et al. catalogues. Carrying out the same analysis of fig. 4 only for sources with flux above 3mJy results
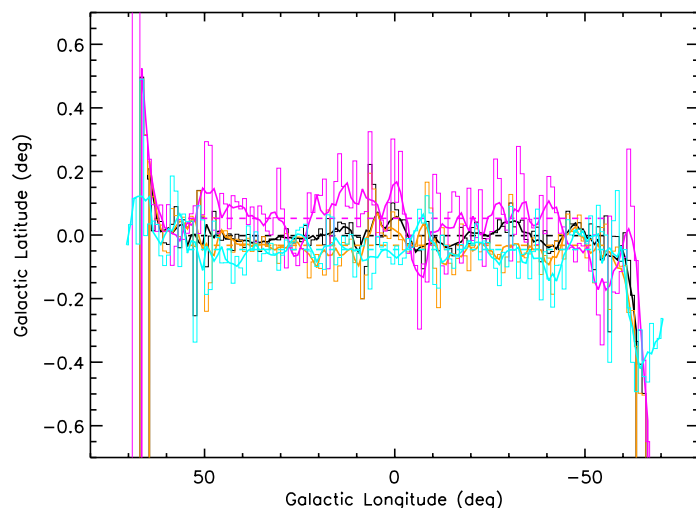
Fig. 9: Same as fig. 4 for the distribution of MIPSGAL 24 μm sources only. The black line is reported straight from fig. 4 for comparison. The orange line represents the distribution again from the Shenoy et al. (in prep) catalogue but for sources with fluxes above 3.5mJy. The cyan line represents the distribution from the WISE 22μm source catalogue with flux above 6 mJy. The magenta line instead represents the distribution of the 24 μm from the catalogue in Gutermuth & Heyer (2015) that are above the respective 90% completeness limit.

in the orange line in fig. 9; this differs somewhat from the black line, but shows again very limited latitude variations around its respective midplane (the orange dashed line), and certainly does not resemble the distribution of the Hi-GAL 70 and 250 μm sources. The same conclusion is reached if we use the WISE 22μm source catalogue; this time we use only sources with flux above ~ 6 mJy, roughly corresponding to the peak of the flux distribution of WISE sources between -60° $\leq l \leq$ 60° and $|b|\leq$ 1, and using the same processing as above we obtain the cyan line in fig. 9. Again the distribution is much flatter around its respective midplane (cyan dashed line) than that of the Hi-GAL sources.

As an additional check, we also used the very recent 24 μm MIPSGAL catalogue of Gutermuth & Heyer (2015) that contains high-reliability objects and very conveniently includes for each source an estimate of the local 90% flux completeness value. We carry out the same analysis again for the Gutermuth & Heyer (2015) catalogue only using sources above the completeness and the result is shown by the magenta line in fig. 9. The latitude variations of the magenta line with respect to its median-determined midplane (the magenta dashed horizontal line) are still substantially limited, and again completely differ from the Hi-GAL sources. There are differences between the latitude distribution of 24 μm sources between Shenoy et al. and Gutermuth & Heyer (2015), but this is beyond the scope of the present paper that is focused on Herschel data.

We conclude that completeness or extinction biases over the entire sample of detected 24μm sources cannot explain the intrinsically different shapes of the longitude distribution of sources' latitude when the entire 24μm catalogues are considered. It is only when the 24μm catalogues are filtered with criteria that preferentially select YSOs that the the 24μm sources distribution more closely approaches the distribution of the Herschel sources.

4. Tracer-dependent disk distortions: evidence for an external agent.

Our results confirm the findings of the studies mentioned earlier (see §1) with much higher reliability and statistical significance, but it is noteworthy that those previous investigations were basically successful in identifying the large-scale latitude modulations in the distribution of gas and star-forming tracers using relatively small or limited data sets.

One fact to recall at this point is the different appearance in the latitude distribution of the Galactic disk as a function of the tracer. For instance, the HI elliptical disk distribution in the CMZ is tilted by ~24° (McClure-Griffiths et al. 2012), i.e significantly more than the inclination angle of ~ 1°.27 that we infer from the median longitude distribution of the latitude centroid of the *Herschel* 500-μm emission via a simple linear fit to the black line in fig. 3 in the range $17°.5 \gtrsim l \gtrsim -10°$.

The different morphology in the latitude distribution of the Galactic disk as a function of the tracer can provide clues concerning the possible agents responsible for driving the perturbations. Alfaro et al. (1992) report modulations along the Sagittarius-Carina arm, not only in the star-formation and gas tracers but also in the young stellar populations traced by young clusters. These deviations have a maximum semi-amplitude of about 50 pc, assuming that the clusters are indeed distributed along the Sag-Car arm between l=20° and l=280° (going through the Galactic Centre). At the heliocentric distance of the Sag-Car arm toward the l=300° line of sight, 50 pc correspond to an angular amplitude of more than 1°.8. Such large amplitude modulations are not measured in the latitude distribution of objects in recent near/mid-IR Galactic Plane Surveys. Benjamin et al. (2005) does not report any distortion of the stellar component traced by the Spitzer/GLIMPSE survey, showing a mean latitude source distribution close to b=0°. The mean latitude distribution of the sources detected in the Spitzer/MIPSGAL 24-μm survey, represented by the black histogram and full thick line in fig. 4, tends to depart from a perfect flat distribution, showing some distortions that seem uncorrelated and of much lower amplitude than in the *Herschel* 70-μm and 250-μm sources; certainly, nothing similar to what proposed by Alfaro et al. (1992) is revealed. We argue that the limited number of clusters (28) used in Alfaro et al. (1992) is not representative of the stellar component of the disk in the Sag-Car arm. To summarize, we are presented with a complex scenario where the latitude distribution of the Galactic disk behaves differently depending on the tracer considered. Latitude modulations as a function of longitude are observed in the atomic and relatively less dense phase of the ISM traced by the HI 21-cm line. The same modulations, with a lower amplitude, are revealed in the denser ISM phase traced both by the large-scale diffuse cold dust emission, and by the distribution of the star-forming clumps revealed at $\lambda \geq 70$ μm in the *Herschel* Hi-GAL survey. No evidence of such modulations are found in the point sources detected by the Spitzer MIPSGAL and, to the best of our knowledge, GLIMPSE surveys, when the entire source samples are considered. If instead we consider the subsample selected based on color criteria targeted toward YSOs as in Robitaille et al. (2008), the distribution exhibits some of the characteristics of the Herschel sources distributions.

It is difficult to interpret this picture by invoking gravitational perturbations induced by the Milky Way satellites, as gravity would indifferently act both on gas and stars, while the distortion here is only seen in diffuse gas and dust and the star-forming component of the Galaxy (but see Carlin et al. 2013). Like-wise, any dynamical perturbation induced by non-axisymmetric agents like the Galactic Bar should act on all disk components as well. A plausible driving agent has to dynamically interact with the diffuse, gas and dust content of the disk but have negligible cross-section with the stellar component. We propose that such an agent may be constituted by incoming flows of relatively low-density diffuse material from the Galactic halo accreting onto the Galactic disk and/or by Galactic fountain gas.

4.1. Interaction between gas flows and the Galactic disk

While a detailed model of the interaction between the Galactic disk and incident extraplanar gas flows is beyond the scope of this paper, it is instructive to verify the plausibility of this interpretation. Approximating the Galaxy as a thin disk of uniform surface density σ_0, the vertical gravitational field at a height z above (or below) the plane can be written as

$$g \approx -2\pi G\sigma_0 \left[1 - \frac{z/R_0}{\sqrt{1 + (z/R_0)^2}} \right] \tag{1}$$

In our specific case we take 0°.2 as a representative distortion amplitude from fig. 4. The linear vertical amplitude z will of course depend on where in the inner Galaxy the distortion is located, but even at the location of the CMZ this would correspond to about 30 pc; this is negligible with respect to whatever choice we make for the Galaxy radius R_0. In other words $z/R_0 \ll 1$, so that the term in square brackets in eq. 1 is ~1. A fraction of the disk of unit area undergoing a vertical distortion above the plane, with amplitude z much smaller than the Galaxy radius, will then experience a downward force

$$F_z \approx -2\pi G\sigma_0^2 \tag{2}$$

in the above we neglect that the field in eq. 1 includes the contribution from the unit area undergoing the distortion. Assuming that the distortion is a stationary feature, this force will have to equal the force exerted by an incoming flow of gaseous material at velocity v_f, that we can write as

$$F_f = \dot{m}_f v_f \tag{3}$$

which, for a unit area flow column, can be rewritten as

$$F_f = \rho_f v_f^2 \tag{4}$$

At equilibrium $F_z = F_f$, so that the required volume density of the incoming flow is

$$\rho_f = \frac{2\pi G\sigma_0^2}{v_f^2} \tag{5}$$

For a typical average velocity of High-Velocity Clouds (REF) of $v_f \sim 200$ km s^{-1}, and a mean Galaxy surface density of $\sigma_0 \sim 0.015$ g cm^{-2} (Bovy & Rix 2013), we obtain $\rho_f \sim 0.077$ cm^{-3}. These volume densities, as approximate as they are in this very simplified treatment, are compatible with measurements of extraplanar gas in Intermediate and High-Velocity Clouds (e.g., Putman et al. 2012 or Shapiro & Benjamin 1991, see below next paragraph).

Such flows would provide an important large-scale momentum input for ordered flows in the disk or to drive turbulence, two of the main mechanisms invoked for the origin of dense ISM clouds and filaments where supercritical conditions for star formation exist (Molinari et al. 2014 and references therein).

4.2. Galactic fountain or accretion from halo flows ?

The large-scale ordered appearance of the distortions revealed by *Herschel* would suggest that these features are stable over fractions of the orbital period. One can ask how this time scale compares with that of such dynamical processes as produced by "Galactic fountains". To drive a Galactic fountain, a series of massive stars from OB associations have to generate supernovae to guarantee that sufficient momentum is available to create a large-scale fountain. Assuming a Salpeter IMF, McCray & Kafatos (1987) estimated that this phase lasts 5×10^7 yrs, on average. When the expelled gas falls back it will impact the Galactic disk that is locally rotating with a tangential velocity of $\sim$220 km s^{-1} basically everywhere in the inner disk.

Direct evidence of this gas mainly comes from UV spectroscopy that Shapiro & Benjamin (1991) modelled with a $n_H \sim 10^{-2}$ cm^{-3} medium accreting onto the Galactic disk over linear extents exceeding a kiloparsec. Assuming that the infalling fountain lasts the same amount of time as the series of supernova explosions, the spatial extent of the interface among the two flows will be in excess of 10 kpc, comparable to the linear extent that we can reasonably project from the angular extent of the observed disk bending (see e.g. Fraternali et al. 2015). The Galactic fountain hypothesis is therefore compatible with the extent of the observed features from a timescale viewpoint.

Accretion onto galaxies from halo gas that is intergalactic in origin is commonly invoked to solve the gas depletion problem in star-forming galaxies. At an average Galactic star-formation rate of $\sim$ 1M$_\odot$ yr^{-1}, the Milky Way would exhaust its current reservoir of molecular gas in about 2×10^9 years, clearly requiring replenishment of fresh ISM material from the surrounding halo; we refer the reader to the recent reviews of Sancisi et al. (2008) and Putman et al. (2012). Fraternali & Tomassetti (2012) suggest that the very existence of a star-formation Schmidt-Kennicutt law requires continuous fuelling of gas, either from gas stripping from orbiting dwarf galaxies or accretion from a diffuse halo. Peek (2009) simulates gas accretion from different sources in the Galactic potential and concludes that accretion from a diffuse halo is able to channel fresh ISM onto the most currently active star-forming Galactocentric radii, while accretion from dwarf satellites gas stripping would be dominant outside of the Solar circle therefore requiring efficient inward gas radial transport. While the latter is possible in principle, the need to transfer angular momentum outward would seem to make the process very inefficient even in the presence of well developed spiral arms (e.g., Peek 2009).

These flows could also correspond to the High-Velocity or Intermediate-Velocity Clouds observed in the HI 21-cm data (Putman et al. 2012), with densities of the order of 0.1 cm^{-3} and line-of-sight-velocities of hundreds of km s^{-1}, again compatible with the values required to cause and maintain local disk distortions (eq. 5). As the disk distortions are mostly seen as bendings toward negative latitudes, the proposed mechanism would require that most of the incoming gas comes from northern Galactic latitudes. Such an asymmetry is indeed observed in extraplanar gas in the major IVCs Marasco et al. (2012) that are believed to be a manifestation of the fountain gas, as well as in the major HVC that in part could be due to halo gas flows.

4.3. Evolution of the distortions

As soon as stars are formed out of the cold and dense clouds their cross-section is reduced, such that they can dynamically decouple from their gaseous environment and rapidly settle down onto the $b = 0°$ midplane. The representative maximum displacement of the barycenter of the diffuse 500-μm emission as well as of the latitude medians of the 70- and 250-μm compact sources with respect to the $b = 0°$ midplane is $\sim 0°.2$. At a distance of 5 kpc, this is a representative value for the portion of Sagittarium Arm undergoing the downward bend in the 1st Quadrant (§3.2.1), and corresponds to about 17 pc. With a vertical velocity of 7 km s^{-1}, comparable to the Sun's vertical speed with respect to the LSR (e.g., Binney & Merrifield 1998), an object would cover this space in about 2.3 Myr. At the $\sim$8.4 kpc distance that we assume on average for the Galactic Bar, where the spectacular $25° \geq l \geq -25°$ sinusoidal-like latitude modulation is seen (§3.2.2b), the vertical displacement would be of the order of 30 pc, requiring $\sim$4 Myr to reach the midplane at the same 7-km s^{-1} vertical speed.

These timescales are compatible with the formation timescale of the low- and intermediate-mass stars that constitute the bulk of the stellar mass in the clusters that form in the Hi-GAL clumps. It is then plausible that the observed distortions in the cold and star-forming component of the Galactic disk can settle down toward the flatter latitude distribution seen for the mix of relatively more evolved YSOs and MS/post-MS objects traced at by MIPSGAL 24μm or WISE 22μm sources, and for the stellar Galactic disk in general. This would be the first direct evidence of a steady star formation from accretion of fresh extraplanar material.

5. Conclusions

The assembly of panoramic views of the inner Milky Way from the *Herschel* Hi-GAL survey enables studies of the spatial distribution in Galactic longitude and latitude of the interstellar medium and of dense star-forming clumps with unprecedented detail and statistical significance.

The width of the Galactic Plane expressed as the FWHM of the latitude distribution of high-reliability Hi-GAL compact sources, with counterpart in at least three adjacent *Herschel* photometric bands, has a mean value of $0°.75$ over the $+60° \geq l \geq -60°$ inner Galaxy. The width of the Plane measured by the FWHM of the diffuse 500-μm emission from dust is about twice as large. The peak of the overall latitude distribution of Hi-GAL sources is at $b \sim -0°.06$, essentially coincident with the results from ATLASGAL.

Large-scale latitude distortions of the Galactic Plane are visible in the $\sim$130°-long 500-μm mosaic presented in fig. 1. A quantitative determination of the peak and width of the latitude distribution of the dust column density has been made via a polynomial fit to the emission in bins of 1° in longitude. Strong star-forming complexes are clipped out to obtain a more reliable determination of the distribution peak in latitude. The width of the distribution is determined by the half-power width of the fit. The number density of compact sources from the band-merged Hi-GAL photometric catalogues is analysed as a function of latitude, by computing the median latitude values for sources in 1°-wide longitude bins. The detailed latitude distribution as a function of longitude shows clear modulations visible, both for the diffuse emission and for the compact sources, as large-scale bending modes over all of the considered longitude range. Bends are mostly toward negative latitudes, with excursions of $\sim 0°.2$

below the midplane in the smoothed distributions peaking at $l \sim$ $+40°$, $+12°$, $-25°$ and $-40°$. The only positive bend peaks at $l \sim -5°$. No comparable modulations can be found in the distributions of the entire samples of MIPSGAL 24-μm or the WISE 22μm point source distribution analysed with the same methodology, and none is reported for the GLIMPSE point-source distribution. The analogous distribution using the subsample of MIPSGAL/GLIMPSE sources selected based on color criteria targeted toward YSOs (Robitaille et al. 2008), exhibits instead some of the features shown by the Herschel sources.

The distortions of the Galactic inner disk revealed by *Herschel* confirm previous findings with much lower statistical significance from CO surveys and HII/OB source counts. The fact that no such distortions are visible with tracers of more evolved YSOs or the stellar disk in general would rule out gravitational instabilities or satellite-induced perturbations, as they should act on both the diffuse and stellar disk components. We propose that incoming flows of diffuse material from the Galactic halo interact with the disk causing the bends seen in the *Herschel* data. These effects are still visible in the distribution of very young star-forming clumps. Stars have a much lower cross-section with the supposed incoming flows, therefore decoupling from them and relaxing onto the stellar disk. The timescale required for the disappearance of the distortions from the diffuse ISM to the relatively evolved YSO stages are compatible with star formation timescales, assuming a velocity equal to the Sun's vertical speed in the disk.

References

Alfaro, E. J., Cabrera-Caño, J., & Delgado, A. J. 1992, ApJ, 399, 576

Anderson, L. D., Bania, T. M., Balser, D. S., et al. 2014, ApJS, 212, 1

Benjamin, R. A., Churchwell, E., Babler, B. L., et al. 2005, ApJ, 630, L149

Beuther, H., Tackenberg, J., Linz, H., et al. 2012, ApJ, 747, 43

Billot, N., Noriega-Crespo, A., Carey, S., et al. 2010, ApJ, 712, 797

Billot, N., Schisano, E., Pestalozzi, M., et al. 2011, å, 735, 28

Binney, J. & Merrifield, M. 1998, Galactic Astronomy, Princeton Series in Astrophysics (Princeton University Press)

Blitz, L., Magnani, L., & Mundy, L. 1984, ApJ, 282, L9

Bovy, J. & Rix, H.-W. 2013, ApJ, 779, 115

Bregman, J. N. 1980, ApJ, 236, 577

Carey, S. J., Noriega-Crespo, A., Mizuno, D. R., et al. 2009, PASP, 121, 76

Carlin, J. L., DeLaunay, J., Newberg, H. J., et al. 2013, ApJ, 777, L5

Contreras, Y., Schuller, F., Urquhart, J. S., et al. 2013, A&A, 549, A45

Csengeri, T., Urquhart, J. S., Schuller, F., et al. 2014, A&A, 565, 75

Elia, D., Molinari, S., Schisano, E., et al. 2015, A&A, in preparation

Franco, J., Kim, J., Alfaro, E. J., & Hong, S. S. 2002, ApJ, 570, 647

Franco, J., Tenorio-Tagle, G., Bodenheimer, P., Rozyczka, M., & Mirabel, I. F. 1988, ApJ, 333, 826

Fraternali, F., Marasco, A., Armillotta, L., & Marinacci, F. 2015, MNRAS, 447, 70

Fraternali, F. & Tomassetti, M. 2012, MNRAS, 426, 2166

Gum, C. S., Kerr, F. J., & Westerhout, G. 1960, MNRAS, 121, 132

Gutermuth, R. A. & Heyer, M. 2015, AJ, 149, 64

Kwak, K., Shelton, R. L., & Raley, E. A. 2009, ApJ, 699, 1775

Liszt, H. S. & Burton, W. B. 1980, ApJ, 236, 779

Lockman, F. J. 1977, AJ, 82, 408

Marasco, A., Fraternali, F., & Binney, J. J. 2012, MNRAS, 419, 1107

Marinacci, F., Binney, J., Fraternali, F., et al. 2010, in American Institute of Physics Conference Series, Vol. 1240, American Institute of Physics Conference Series, ed. V. P. Debattista & C. C. Popescu, 166

Matthews, L. D. & Uson, J. M. 2008, ApJ, 688, 237

McClure-Griffiths, N. M., Dickey, J. M., Gaensler, B. M., et al. 2012, ApJS, 199, 12

McCray, R. & Kafatos, M. 1987, ApJ, 317, 190

Molinari, S., Bally, J., Glover, S., et al. 2014, in Protostars and Planets V, ed. H. Beuther, R. Klessen, C. P. Dullemond, & T. Henning (University of Arizona Press), 125

Molinari, S., Schisano, E., Elia, D., et al. 2015, A&A, submitted

Mookerjea, B., Kramer, C., Nielbock, M., & Nyman, L. 2004, A&A, 426, 119

Peek, J. E. G. 2009, ApJ, 698, 1429

Piazzo, L., Calzoletti, L., Faustini, F., et al. 2015, MNRAS, 447, 1471

Piazzo, L., Ikhenaode, D., Natoli, P., et al. 2012, IEEE Transactions on Image Processing, 21, 3687

Pranav, P. & Jog, C. J. 2010, MNRAS, 406, 576

Putman, M. E., Peek, J. E. G., & Joung, M. R. 2012, ARA&A, 50, 491

Quiroga, R. J. 1974, Ap&SS, 27, 323

Robitaille, T. P., Meade, M. R., Babler, B. L., et al. 2008, AJ, 136, 2413

Rosolowsky, E., Dunham, M. K., Ginsburg, A., et al. 2010, ApJS, 188, 123

Sancisi, R., Fraternali, F., Oosterloo, T., & van der Hulst, T. 2008, Astron. & Astroph. Review, 15, 189

Santillán, A., Franco, J., Martos, M., & Kim, J. 1999, ApJ, 515, 657

Shapiro, P. R. & Benjamin, R. A. 1991, PASP, 103, 923

Spitzer, L. 1990, ARA&A, 28, 71

Traficante, A., Calzoletti, L., Veneziani, M., et al. 2011, MNRAS, 416, 2932

Vaidya, B., Hartquist, T. W., & Falle, S. A. E. G. 2013, MNRAS, 433, 1258

Wakker, B. P. & van Woerden, H. 1991, A&A, 250, 509

Weiland, J. L., Blitz, L., Dwek, E., et al. 1986, ApJ, 306, L101

Weinberg, M. D. 1991, ApJ, 373, 391